XLIII CILAMCE
21–25, November, 2022
FOZ DO IGUAÇU – PR – BRAZIL

Full-interaction design of composite ribbed lattice girder slabs with cold-formed lipped channel shuttering

Lucas Fadini Favarato[1,2*]André Vasconcelos Soares Gomes[1,2], Daniel Carvalho de Moura Candido[2], Johann Andrade Ferrareto[3], Juliana da Cruz Vianna[2], Adenilcia Fernanda Grobério Calenzani[2]

[1]*Construction Development Area, ArcelorMittal Brazil*
Brigadeiro Eduardo Gomes Avenue, 526, 29.160-904, Serra/ES, Brazil
lucas.favarato@arcelormittal.com.br, lucasffavarato@gmail.com, andre.vs.gomes@arcelormittal.com.br
[2]*Civil Engineering Graduate Program, Federal University of Espírito Santo*
Fernando Ferrari Avenue, 514, 29075-910, Vitória/ES, Brazil
danielcandido89@gmail.com, jcvianna30@gmail.com, afcalenzani@gmail.com
[3]*ArcelorMittal Construction, Constructive Systems Department*
Loute de la Forge, 16, 55000, Haironville, France
johann.ferrareto@arcelormittal.com
**Main author*

Abstract. The development of design methods for steel-concrete composite slabs grew in importance due to an ever-increasing demand for architectural flexibility, which allows for the reduction of total construction cost and simplifies construction procedures. An alternative to traditional pre-cast lattice joist slabs was recently developed, which implements a cold formed steel (CFS) profile fastened to trussed rebar by uniformly distributed plastic spacers. Previous theoretical studies resulted in methods for predicting the ultimate allowable live load of this slab system. However, steel-concrete composite behavior was neglected due to the absence of experimental data. As such, this paper relies on standardized design codes to propose a design method that accounts for composite behavior, considering full interaction between CFS profile and reinforced concrete (RC). Altogether, the results obtained have evidenced a better performance of the system regarding the previous design methods, expressed by the increase of unpropped span in more than 80%.

Keywords: composite ribbed slab, full composite action, resistance.

1 Introduction

Composite slabs were first developed in the United States during the 1940's. These systems were composed by a cold-formed steel (CFS) profile (steel decking) intended to behave in structural unison with reinforced concrete (RC). Said composite behavior is induced by shear transfer mechanisms located at material interface, to combat relative displacement between materials. This structural configuration resulted in significant weight reduction if compared to slabs composed purely of RC, which were the predominant choice for floor systems at the time (CRISINEL; O'LEARY, 1996).

Since then, the development of different composite floor systems has greatly contributed to reduce the weight of high-rise steel buildings. The introduction of new systems became more significant as a result of an increasing demand for structural elements capable of spanning greater distances and increasing the open area between columns (AHMED; TSAVDARIDIS, 2019). BRAUN *et al.* (2009), for instance, conducted a technical viability study of a structural system able to cover 14 m spans, which allowed a column-free area of 140 m². The system used composite beams and slabs and is commonly known as Composite Slim Floor (CoFSB).

Benefits of composite structures include reduced construction time; reduction of transportation costs;

sustainability; easier installation of plumbing and electrical systems (COUCHMAN; MULLETT; RACKHAM, 2009); increased quality of craftmanship, as well as reduced formwork and material waste (VIANNA, 2005). In contrast, composite floor systems demand a larger number of secondary beams when no shoring is used due to span limitations before concrete curing, in addition to an aesthetic necessity of using suspended lining (SIEG, 2015).

In recent decades, numerous studies concerning composite slab behavior were developed. These studies were aimed at perfecting structural solutions that were poorly explored by the market and frequently ignored by standardized design specifications, or proposing design methods that increase structural efficiency. In this context, the study performed by TAKEY (2001) is highlighted, which consisted of the numerical geometric optimization of an inverse trapezoidal CFS profile, followed by full-scale flexure experiments of five slab specimens with self-fastening screws as the shear transfer mechanism. The results were compared with design standards and indicate that the proposed system is viable. VIANNA (2005) proposes an alternative cross-section geometry to that of TAKEY (2001) and, in addition to the numerical optimization and flexure tests to asses failure modes and ultimate resistance, the study also included pull-out tests to determine the ultimate load that induces relative displacement at material interface. The research is concluded with a technical and economic competitiveness analysis of the slab system. GROSSI (2016) proposed design formulas for composite slabs with additional rebar, based on an extension of normative recommendations for slabs with minimum required rebar. The study focused on developing design procedures for the ultimate limit states of bending moment and longitudinal shear, as well as the serviceability limit state of excessive deformation. Experimental tests were conducted to validate the proposed formulae, and the floor system exhibited increased ductility and resistance.

The company ArcelorMittal recently developed a steel–concrete composite ribbed unidirectional slab system that utilizes a CFS stiffened “U” profile, subjected to minor axis bending. The system combines the underlying principles of composite ribbed slabs and lattice joist slabs in a single product, named Trelifácil® (ARCELORMITTAL, 2017). The traditional precast reinforced concrete (RC) lattice joists are replaced with trussed rebar, fastened inside a CFS profile by uniformly distributed plastic spacers, as shown in Figure 1. Furthermore, the empty spaces between joists are filled with inert elements such as expanded polystyrene (EPS) or ceramic blocks, overlaid with concrete.

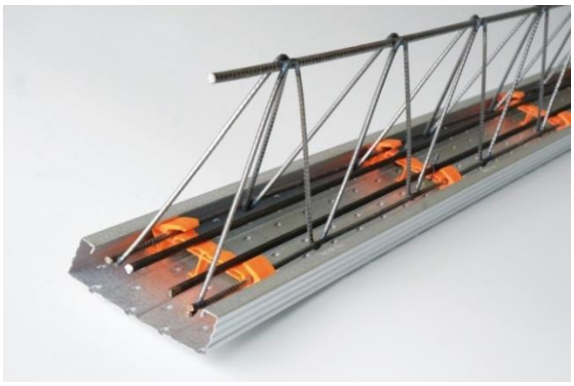

Figure 1. General view of the composing elements of the Trelifácil® joist.
Source: ARCELORMITTAL (2017).

FAVARATO *et al.* (2019) proposed a simplified analytical procedure to determine the ultimate strength of this slab system. However, the design method neglects structural contributions provided by the CFS profile after concrete curing, as well as the combined behavior of all joist elements (profile, truss and spacers) during the construction phase. Although the results obtained with this method indicate strong limitations of assembly without shoring, ultimate design loads show reasonable values from a technical standpoint.

As such, the present study aims to expand the aforementioned method by proposing a novel design procedure for Trelifácil® that considers full composite interaction between RC and the CFS profile in each rib. The study also includes a comparative analysis focused on the minimum and maximum ultimate resistance, with and without composite behavior, respectively.

2 Design of steel-concrete composite ribbed slabs with additional rebar

The design of composite slabs with additional rebar implemented on this paper was based on the European standard (EN 1994-1-1, 2004) and the study conducted by GROSSI (2016). The cross-section geometry of the CFS profile used on Trelifácil® slabs is represented in Figure 2. The thickness of the steel profile is $t_s = 0.65\ mm$.

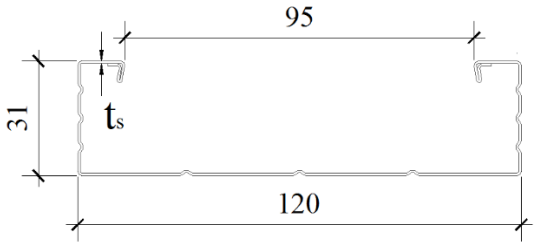

Figure 2. Cross-section geometry of the steel profile. Dimensions in millimeters.
Source: FAVARATO *et al.* (2019).

The results later shown in this paper must be interpreted considering the following assumptions: (i) full composite action between CFS profile and concrete, such that longitudinal shear is not the governing mode of failure; (ii) trussed rebar and CFS profile have identical vertical displacement at the points where plastic spacers are introduced; (iii) redistribution of ultimate design load between trussed rebar and CFS profile, proportional to their rigidities, disregarding possible rupture of the spacers; (iv) the connection of the truss to the profile is not sufficient to avoid buckling of the profile during the construction phase; (v) the ribs are designed as juxtaposed "T" beams and their cross-section geometry depends on the dimensions of inert elements; (FAVARATO et al., 2019); (vi) additional rebar may be included to increase flexural resistance of the final slab; and (vii) during construction, the system composed by the truss and the profile are subjected to the full dead load associated with this phase, in additional to a live load of $1\ kN/m^2$ (EN 1991-1-6, 2005). In closure, it is important to note that propped construction design is beyond the scope of the present analysis.

2.1. Design after concrete curing

The formulae used in this analysis was largely based on those proposed by GROSSI (2016). The method is an extension of the design prescriptions of (EN 1994-1-1, 2004) and (ASSOCIAÇÃO BRASILEIRA DE NORMAS TÉCNICAS, 2008) for the design of steel-concrete composite slabs with no additional rebar. For the scenarios considered, the additional rebar was placed below the compressed concrete layer, considering that the governing limit state was reached before yielding of the additional rebar.

2.1.1 Design after concrete curing

To calculate the ultimate bending moment resistance, consider the "T" section of the composite ribbed slab with additional rebar shown in Figure 3.

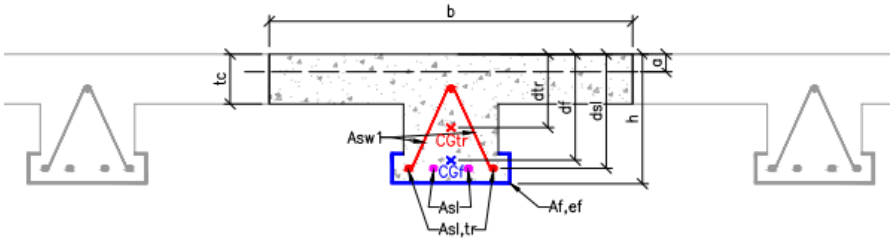

Figure 3. Cross-section of composite ribbed slab with additional rebar.

First, the compressive force N_{cf} acting on the concrete layer of thickness t_c is assessed, along with net forces N_{pa} and N_{sl} acting on the CFS profile and the trussed rebar, respectively. These quantities are obtained with Eq. (1), (2) and (3).

$$N_{cf} = 0.85\ b\ t_c\ f_{cd} \tag{1}$$

$$N_{pa} = A_{F,ef}\ f_{yFd} \tag{2}$$

$$N_{sl} = A_{sl} f_{yd} + A_{sl,tr} f_{yd,tr} \tag{3}$$

in which b is the flange width of the reinforced concrete T section; f_{cd} is the design compressive strength of concrete; $A_{F,ef}$ is the effective cross-section area of the profile, without accounting for embossments; f_{yFd} is the design yield stress of the CFS profile (340 MPa); A_{sl} is the total cross-sectional area of additional rebar; $A_{sl,tr}$ is the total cross-sectional area of the inferior bars of the lattice girder ; f_{yd} is the design yield stress of additional rebar steel; and $f_{yd,tr}$ is the design yield stress of the trussed rebar.

If $N_{cf} > N_{pa} + N_{sl}$, observed as the most common occurrence for this type of slab. This is a result of the relative dimensions between profile and concrete cross-sections, which induces the plastic neutral line (PNL) to be located within the thickness t_c. As such, the exact position "a" of the PNL, measured perpendicular to the upper surface of the slab, may be obtained with Eq. (4):

$$a = \frac{N_{pa} + N_{sl}}{0.85\ f_{cd}\ b} \tag{4}$$

Finally, ultimate bending moment resistance is determined by Eq. (5):

$$M_{Rd} = N_{pa}(d_F - 0{,}5a) + N_{sl}(d_{sl} - 0.5a) \tag{5}$$

In which d_F and d_{sl} are the distances from the upper surface of the slab to the geometric center of the effective cross-section of the CFS profile, and to the geometric center of additional rebar, respectively.

2.1.2 Vertical shear resistance

Vertical shear capacity ($V_{v,Rd}$) is determined with Eq. (6), adapted from (EN1992-1-1, 2004):

$$V_{v,Rd} = V_{v,f,Rd} + V_{v,c,Rd} + V_{sw} \leq V_{Rd,max} \tag{6}$$

As prescribed by (EN1992-1-1, 2004), vertical shear capacity of concrete, $V_{v,c,Rd}$ is obtained from Eq. (7) through (10).

$$V_{v,c,Rd} = \frac{0.18}{\gamma_c} k (100 \rho_1 f_{ck})^{1/3} A_v \geq \nu_{min} A_v \tag{7}$$

$$\rho_1 = \frac{A_s}{A_v} \leq 0{,}02 \tag{8}$$

$$k = 1 + \sqrt{\frac{200}{d}} \leq 2.0, \text{d em mm} \tag{9}$$

$$\nu_{min} = 0.035 k^{\frac{3}{2}} f_{ck}^{\frac{1}{2}} \tag{10}$$

In which $\gamma_c = 1.4$; d is the distance from the upper surface of the concrete layer to the geometric center of the longitudinal tensioned rebar; f_{ck} is the characteristic compressive strength of concrete, in MPa; A_v is the area

of concrete that is subjected to shear force, estimated as $9{,}5d$, in cm²; and A_s is the total area of longitudinal tensile rebar within A_v.

The shear capacity of the steel profile $V_{v,f,Rd}$, is determined by Eq. (11), in accordance with (EN1993-1-3, 2006).

$$\mathrm{V_{v,f,Rd}} = \frac{2h_w}{\operatorname{sen}\phi}\frac{tf_{bv}}{\gamma_a} \tag{11}$$

Here, h_w is the height of the web, measured as the perpendicular distance between the centerline of each flange; ϕ is the angle between web and flange; t is the thickness of the steel profile; f_{bv} is shear strength of the web, considering the incidence of buckling; and γ_a is a resistance factor taken as 1.1. The multiplication by 2 in Eq. (11) is introduced to account for both flanges of the profile subjected to minor axis bending. In other words, the flanges are subjected to forces commonly observed in profile webs.

For the composite slab under analysis, the shear strength of the trussed rebar V_{sw} must also be considered, as indicated in Figure 3. This parameter may be obtained from Eq. (12), adapted from (EN1992-1-1, 2004).

$$\mathrm{V_{sw}} = 2\frac{\mathrm{A_{sw1}}}{\mathrm{p}}0.9\mathrm{d}(\mathrm{cotg}\alpha + \mathrm{cotg}\theta)\mathrm{sen}\alpha\ \mathrm{sen}\beta\ \mathrm{f_{yd}} \tag{12}$$

in which A_{sw1} is the cross-section area of a single bar of the truss; p is the pace of the truss; d is the effective depth; α and β are truss angles measured as shown in Figure 4; θ is the inclination of shear plane on the concrete; and f_{yd} is the yield strength of rebar.

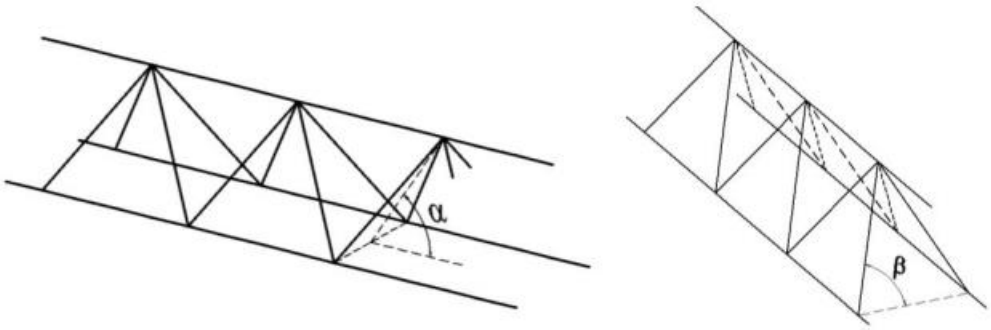

Figure 4. Inclination angles of the truss.
Source: FAVARATO *et al*. (2020).

Finally, the maximum vertical shear force $\mathrm{V_{Rd,max}}$, limited by the crushing of the compressed concrete diagonals, is obtained with Eq. (13).

$$\mathrm{V_{Rd,max}} = \frac{0.54\mathrm{b_w}df_{cd}}{1+\cot^2\theta}(\cot\theta + \cot\alpha) \tag{13}$$

In which b_w is the web thickness, taken as 95 mm; d is the effective depth; f_{cd} is the design compressive strength of concrete.

2.1.3 Vertical displacement

To obtain vertical displacements, first the depth of the neutral line y_{fc} (Figure 5) and the moment of inertia of the composite section I_{fc} must be determined. According to GROSSI (2016), the method that considers crack opening on concrete is the most accurate.

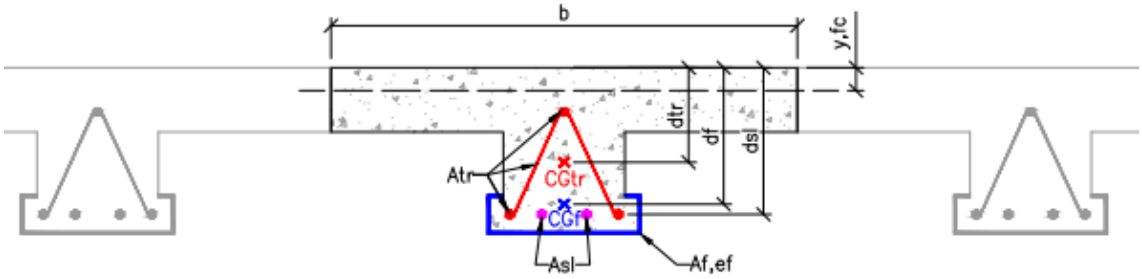

Figure 5. Geometric parameters to determine design properties of the composite cross-section.

The following equations are used:

$$I_{fc} = \left(\frac{b\, y_{fc}^3}{3}\right)\frac{1}{\alpha_E} + I_{F,ef} + A_{F,ef}(y_{fc} - d_F)^2 + n_{sl}\frac{\pi\emptyset^2}{4}\left[\frac{\emptyset^2}{16} + (y_{fc} - d_{sl})^2\right] + I_{tr} + A_{tr}(y_{fc} - d_{tr})^2 \quad (14)$$

$$y_{fc} = d_F\left[-\frac{\alpha_E}{b\, d_F}(A_{F,ef} + A_{sl}) + \sqrt{\frac{\alpha_E^2}{b^2 d_F^2}(A_{F,ef} + A_{sl})^2 + \frac{2\alpha_E}{b d_F}\left(A_{F,ef} + A_{sl}\frac{d_{sl}}{d_F}\right)}\right] \leq t_c \quad (15)$$

$$\alpha_E = \frac{E_a}{E_c} \quad (16)$$

Here, y_{fc} is the perpendicular distance between the neutral line and the upper surface of the slab, considering cracks on the material; $I_{F,ef}$ is the effective moment of inertia of the profile; I_{tr} is the moment of inertia of the trussed rebar; d_{tr} is the distance between the geometric center of the truss to the upper surface of the slab; α_E is the ratio between the elasticity moduli of steel E_a, and concrete E_c; n_{sl} us the number of additional reinforcement steel bars; $\emptyset$ is the diameter of the additional; A_{tr} is the total cross-sectional area of the longitudinal bars of the truss.

The maximum vertical displacement of a simply supported slab subjected to a uniformly distributed load is obtained with Eq. (17), respecting the limit imposed by Eq. (18).

$$\delta_{máx} = \frac{5(qb)L^4}{384 E_a I_{fc}} \quad (17)$$

$$\delta_{lim} = \frac{L}{350} \quad (18)$$

In which q is the load value per unit area; L is the length of the span parallel to the ribs; and the remaining variables are as previously defined.

2.2. Design during construction

Prior to concrete reaching 75% of its cured compressive strength, the structure behaves according to design assumption (vii). Although the load is directly applied on the CFS profile, the trussed rebar is also responsible for resisting a portion of the load. Given design assumption (ii), horizontal sliding between truss and profile is allowed, resulting in the appearance of two distinct neutral lines.

2.2.1. Finite element structural analysis

The maximum allowable loads acting on the truss and CFS profile, assembled according to Figure 6, were determined by the Finite Element Method (FEM), implemented with *Visual Basic for* Applications (VBA). The structure was modelled using one-dimensional elements with two degrees of freedom per node – vertical

displacement and rotation, while the transfer mechanism for vertical forces was modelled with a single degree of freedom – vertical displacement.

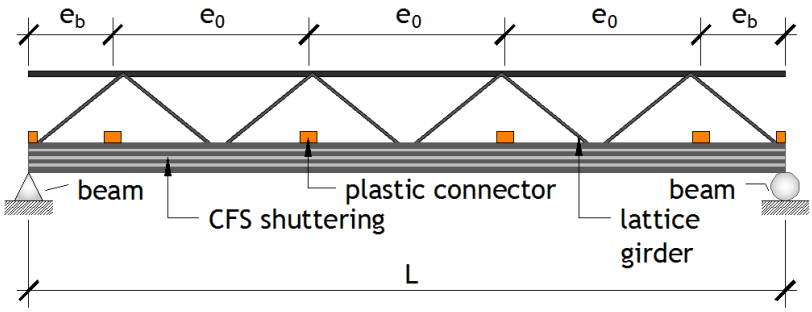

Figure 6. Trussed rebar fastened to the CFS profile.

Since spacers are introduced every 33 cm ($e_0 = 33\ cm$), the distance between the first or last spacer and the closest support of the profile is obtained with Eq. (19) and (20), in which n_c is the number of connectors between supports, rounded down.

$$n_c = \left(\frac{L}{e_0}\right) + 1 \tag{19}$$

$$e_b = \frac{L - e_0(n_c - 1)}{2} \tag{20}$$

The uniformly distributed load is applied directly on the CFS profile and vertical forces are transferred to the truss only at the nodes, i.e., at the points where plastic spacers are introduced. As such, the finite element mesh has a total of $2(n_c + 2)$ nodes, half of which are part of the profile and the remainder is part of the truss. The local stiffness matrix of each beam element is given by Eq.(21), where E_e is the modulus of elasticity of each element; I_e is the moment of inertia about the flexure axis; and L_e is the length of the element (e_0 or e_b).

$$K_{viga,l} = \frac{E_e I_e}{L_e^3}\begin{bmatrix} 12 & 6L_e & -12 & 6L_e \\ 6L_e & 4L_e^2 & -6L_e & 2L_e^2 \\ -12 & -6L_e & 12 & -6L_e \\ 6L_e & 2L_e^2 & -6L_e & 4L_e^2 \end{bmatrix} \tag{21}$$

In addition to only one degree of freedom, the vertical force transfer elements have an axial stiffness of $E_e A_e$ and their local stiffness matrix is shown by Eq. (22). As such, the vertical displacements of the nodes located on the CFS profile are identical to those on the truss, but distinct rotations may be observed.

$$K_{treliça,l} = \frac{E_e A_e}{L_e}\begin{bmatrix} 1 & -1 \\ -1 & 1 \end{bmatrix} \tag{22}$$

The global stiffness matrices of the steel profile (K_{pa}) and trussed rebar (K_{ta}) are of the same order, but with different material properties. Hence, the global stiffness matrix attributed to the entire system (profile and truss) is expressed in Eq. (23) as a function of K_{pa} and K_{ta}, with adjustments to join the degrees of freedom.

$$\begin{bmatrix} K_{pa} & 0 \\ 0 & K_{ta} \end{bmatrix}\{d\} = \{F\} \tag{23}$$

In which $\{d\}$ represents the nodal displacement vector and $\{F\}$ is the global load vector acting on the system. Lastly, if n_c is an odd number, the maximum displacement will occur on the midspan node. Alternatively, if n_c is even, the maximum displacement is obtained by integration of the elastic line on the central element.

2.2.2. Ultimate limit state of the CFS profile associated with bending moment and shear force

For this part of the design procedure, the direct resistance method was used (AUSTRALIA; ZEALAND, 2005; INSITUTE, 2016), due to its ease of application. Three ultimate limit states are considered, as follows.

Lateral torsional buckling (LTB), in accordance to Eq. (24) and (25):

$$\lambda_0 = \left(\frac{\mathrm{Wf_y}}{\mathrm{M_e}}\right)^{0.5} \tag{24}$$

$$\mathrm{M_{Re}} \leq \begin{cases} \mathrm{Wf_y} & \lambda_0 \leq 0.6 \\ 1.11(1 - 0.278\lambda_0^2)\mathrm{Wf_y} & 0.6 < \lambda_0 < 1.336 \\ \dfrac{\mathrm{Wf_y}}{\lambda_0^2} & \lambda_0 \geq 1.336 \end{cases} \tag{25}$$

In which λ_0 is the reduced slenderness associated with LTB; W is the elastic modulus of the gross cross-section; f_y the yield strength of steel; M_e is the bending moment that causes elastic buckling; and M_{Re} is the characteristic bending moment strength of LTB.

Local buckling (LB), in accordance with Eq. (26) and (27):

$$\lambda_\mathrm{l} = \left(\frac{\mathrm{M_{Re}}}{\mathrm{M_l}}\right)^{0.5} \tag{26}$$

$$\mathrm{M_{Rl}} \leq \begin{cases} \mathrm{M_{Re}} & \lambda_\mathrm{l} \leq 0.776 \\ \dfrac{\mathrm{M_{Re}}}{\lambda_\mathrm{l}^{0.8}}\left(1 - \dfrac{0.15}{\lambda_\mathrm{l}^{0.8}}\right) & \lambda_\mathrm{l} > 0.776 \end{cases} \tag{27}$$

In which λ_l is the reduced slenderness associated with LB; M_l is the bending moment that causes elastic LB; and M_{Rl} is the characteristic bending moment strength associated with LB.

Distortional buckling (DB), in accordance with Eq. (28) and (29):

$$\lambda_{\mathrm{dist}} = \left(\frac{\mathrm{Wf_y}}{\mathrm{M_{dist}}}\right)^{0.5} \tag{28}$$

$$\mathrm{M_{Rdist}} \leq \begin{cases} \mathrm{Wf_y} & \lambda_{\mathrm{dist}} \leq 0.673 \\ \dfrac{\mathrm{Wf_y}}{\lambda_{\mathrm{dist}}}\left(1 - \dfrac{0.22}{\lambda_{\mathrm{dist}}}\right) & \lambda_{\mathrm{dist}} > 0.673 \end{cases} \tag{29}$$

In which λ_{dist} is the reduced slenderness associated with DB; M_{dist} is the bending moment that causes elastic DB; and M_{Rdist} is the characteristic bending moment strength associated with DB.

The design resistant bending moment, $M_{p,Rd}$, is the smallest of values obtained from Eq. (25), (27) and (29), subjected to a resistance reduction factor $\gamma_a = 1.10$. The bending moments associated with each elastic buckling mode were obtained with numerical analyses conducted with ANSYS by FAVARATO et al. (2019).

The design resistance to shear force is obtained with Eq. (11). Structural safety of the CFS profile during construction is ensured if the conditions expressed in Eq. (30) and (31) are met.

$$\frac{\mathrm{M_{p,sd}}}{\mathrm{M_{p,Rd}}} \leq 1 \tag{30}$$

$$\frac{\mathrm{V_{p,sd}}}{\mathrm{V_{p,Rd}}} \leq 1 \tag{31}$$

2.2.3. Resistance to concentrated loads

In accordance with (FAVARATO et al., 2019) and (FAVARATO et al., 2020), the CFS profile must resist to concentrated load applied as reactions. Controlling this ultimate limit state, hence, failure of non-stiffened webs due to compression is avoided. As such, the resistance is defined by ABNT NBR 14762 (ASSOCIAÇÃO BRASILEIRA DE NORMAS TÉCNICAS, 2010) and it must be calculated according to Eq. (32).

$$\mathrm{F_{wc,Rd}} = \frac{\alpha \mathrm{t_w^2 f_y} \operatorname{se\,n}\,\varphi}{1.35}\left(1 - \alpha_\mathrm{r}\sqrt{\frac{\mathrm{r_i}}{\mathrm{t_w}}}\right)\left(1 + \alpha_\mathrm{c}\sqrt{\frac{\mathrm{c}}{\mathrm{t_w}}}\right)\left(1 - \alpha_\mathrm{h}\sqrt{\frac{\mathrm{h_w}}{\mathrm{t_w}}}\right) \tag{32}$$

Where t_w is the thickness of web; α takes into account the load case and flange condition; c is the bearing length; φ is the angle between the bearing surface and the plane of the web, taken as 90º; f_y is the steel design strength; r_i is the internal bending radius; α_r, α_c and α_h are standardized coefficients that depend on the internal bending radius, bearing length and web slenderness, respectively; and h_w is the flat length of web measured in its plane.

2.2.4. Maximum displacement of the CFS profile during construction

To obtain the displacements, the moment of inertia of the gross section $\mathrm{I_g}$, must be reduced to an effective moment of inertia, $\mathrm{I_{ef}}$. For the direct strength method, this reduction is performed by implementing Eq. (33).

$$\mathrm{I_{ef}} = \mathrm{I_g}\left(\frac{\mathrm{M_{R_{ser}}}}{\mathrm{M_n}}\right) \leq \mathrm{I_g} \tag{33}$$

In the equation presented above, M_n is the design bending moment acting on the structure, obtained from load combinations associated to serviceability limit states; and $M_{R_{ser}}$ the serviceability bending moment, obtained with Eq. (24) to (29), and substituting Wf_y by M_n. Furthermore, ponding effects must also be considered on the design procedure. As such, if the maximum displacement of the CFS profile at midspan exceeds $L/250$, the thickness of the concrete layer must be incremented by 70% of the original thickness. The maximum displacement obtained after this adjustment must not exceed either $L/180$ or $2\ cm$.

2.2.5. Structural safety of trussed rebar

The ultimate limit states of the trussed rebar must also be verified during the construction phase. The first of which is the buckling or compressive yield of the compressed bars of the truss, brought about by the presence of bending moment. The ultimate bending moment resistance $M_{t,Rd,bs}$, is obtained with Eq. (34).

$$\mathrm{M_{t,Rd,bs}} \leq \begin{cases} \dfrac{\pi^2 \mathrm{E_t}}{\mathrm{k^2 p^2}}\left[\dfrac{\pi(\emptyset S)^4}{64}\right]\dfrac{\mathrm{H_t}}{\gamma_s} \\ f_{t,yk}\left[\dfrac{\pi(\emptyset S)^2}{4}\right]\dfrac{\mathrm{H_t}}{\gamma_s} \end{cases} \tag{34}$$

In which H_t is the height of the truss; γ_s is the resistance factor associated with rebar steel, taken as 1.15; E_t is the modulus of elasticity of truss steel, taken as 210 GPa; k is the buckling coefficient, conservatively chosen as 1.0 (GASPAR, 1997); p is the pace of the truss; $\emptyset S$ is the diameter of the upper bar of the truss; and $f_{t,yk}$ is the yield strength of truss steel, taken as 600 MPa (CA-60).

Sequentially, the design bending moment that induces yielding of the lower bars of the truss may be obtained by using Eq. (35).

$$M_{t,Rd,ebi} = \left[\frac{\pi(\emptyset I)^2}{2}\right]\frac{f_{t,yk}}{\gamma_s} H_t \tag{35}$$

In which $\emptyset I$ is the diameter of a single lower bar.

Lastly, the force that causes the yielding of the diagonal bars $V_{t,Rd,edt}$,must be determined. Equilibrium of vertical forces results in Eq. (36).

$$V_{t,Rd,edt} = \left[\frac{\pi(\emptyset D)^2}{2}\right]\frac{f_{t,yk}}{\gamma_s} \text{sen}\,\alpha\,\text{sen}\,\beta \tag{36}$$

Here, α and β are taken as previously shown in Figure 4; and $\emptyset D$ is the diameter of the diagonal bars of the truss.

3 Results and discussions

To show how the design methodology developed herein fares in comparison with the one proposed by FAVARATO et al. (2019), the same pair of case studies from that research are reproduced here (Table 1). The focus of the comparison is maximum allowable live load and maximum unpropped span for a given set of structural parameters. The characteristics shared by both cases are the following: characteristic compressive strength of concrete chosen as 25 MPa; truss model TR8645, with a yield strength of 600 MPa; inert elements with a specific weight of 0.37 kN/m³; 2 additional rebars with a diameter of 6.3 mm, CA-50 ($f_{yk} = 500\ MPa$); yield strength of profile steel of 340 MPa; and profile thickness of 0.65 mm. The parameters that vary between the two cases are given below.

a) Case 1: concrete layer with 5 cm thickness and inert elements with a 27×8 cm cross-section.
b) Case 2: concrete layer with 6 cm thickness and inert elements with a 37×8 cm cross-section.

Table 1. Input data for analysis (adapted from (FAVARATO et al., 2020)).

Data type	Parameter	Value	Unit
GENERAL DATA	Shuttering yield strength	340	MPa
	Concrete compressive strength	25	MPa
	Lattice girder model	TR8645	--
	Lattice girder yield strength	600	MPa
	Additional rebar	2Ø6.30	mm
	Additional rebar yield strength	500	MPa
	Light filling material density	0.37	kN/m³
SCENARIO 1	Concrete layer thickness	5	cm
	Blocks dimensions	27 x 8	cm
SCENARIO 2	Concrete layer thickness	6	cm
	Blocks dimensions	37 x 8	cm

The following caption was used to graphically represent each limit state analyzed: p-BM-BC – bending moment resistance of CFS profile, before curing; p-VS-BC – shear force resistance of CFS profile, before curing; p-WC-BC – crushing of CFS profile web, before curing; lg-UCB-BC – buckling of upper bar of the truss, before curing; lg-LCY-BC – yield of lower truss bars, before curing; lg-DY-AC – yield of diagonal truss bars, before curing; D-BC – deflection, before curing; BM-AC – bending moment resistance, after curing; VS-AC – vertical shear resistance, after curing; D-AC – deflection, after curing; and CW-DC – crack opening, after curing, applicable only when the slab is designed as a RC slab.

3.1. Case 1

The results are shown in Figure 7. Note that shear resistance was the governing limit state for short to moderate spans, up to 1.40m. For longer spans, maximum deflection was the governing design parameter. Furthermore, the ultimate limit state associated with bending moment was not critical in any of the spans analyzed. In comparison with the values obtained from FAVARATO et al. (2019), the maximum span in which shear force resistance was the governing mode of failure increased from 1.00 m to 1.40 m. Moreover, on the study conducted by FAVARATO et al. (2019), the crushing of concrete at the top of "T" section was a critical mode of failure for spans of up to 1.20 m, this behavior is not observed with the new methodology.

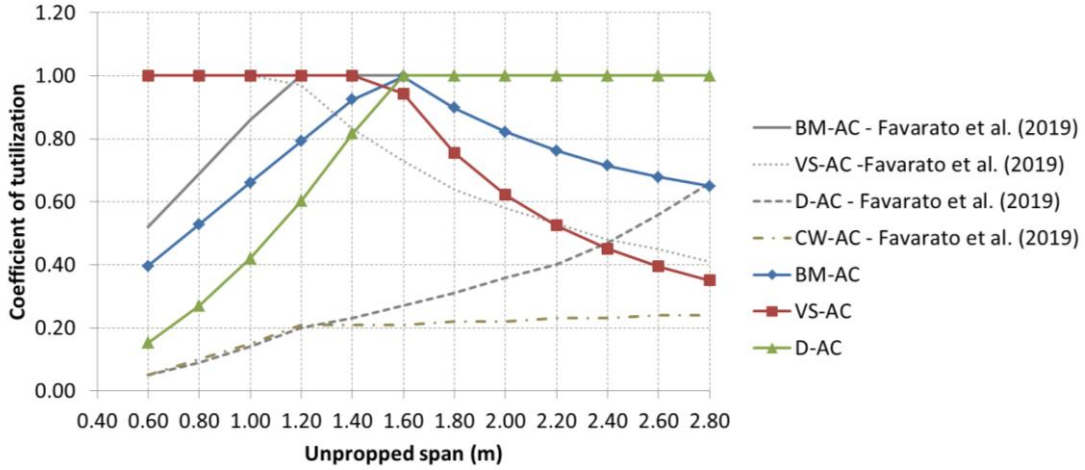

Figure 7. Results for Case 1 – after curing.

Concerning maximum unpropped span (Figure 8), substantial increase is observed in relation with the previous methodology, from 1.20 m to 2.10 m, which corresponds to 75%, limited by buckling of the truss bar under compression. This a result of an increase in flexural rigidity provided to the system when equal vertical displacement is considered at the point of introduction of plastic spacers. On the other hand, although the upper bar of the truss has some contribution to the bending moment resistance of these slabs, said contribution is small enough to be disregarded. As such, the buckling of the upper bar of the truss is allowable during construction, and the determining factor of maximum unpropped span becomes maximum deflection. With this consideration, the maximum allowable unpropped span is increased to 2.20 m, corresponding to an 83% increase if compared to the design procedure that disregards any contribution provided by the trussed rebar. Therefore, the buckling of the compressed bar of the truss is more sensitive than yielding of profile steel or buckling of the profile, since a larger portion of the load is resisted by the element with more rigidity, the truss.

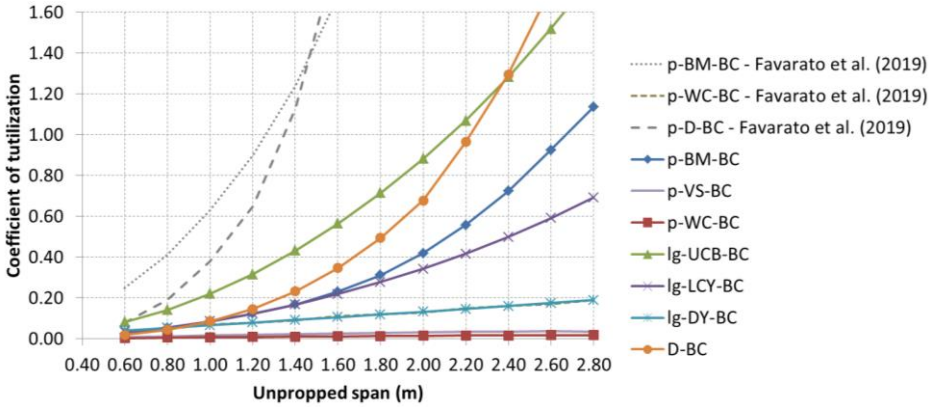

Figure 8. Results for Case 1 – before curing.

3.2. Case 2

Figure 9 presents the results for Case 2. Similar conclusions are drawn concerning the limit states: Vertical shear resistance governs design for spans up to 1.6m, which represents a 14% increase in comparison with the previous methodology. This behavior may be attributed to an increase in effective depth and in shear area. Displacement becomes a limiting factor for spans greater than or equal to 2.00 m, due to the increased flexural rigidity provided by the larger flange of the "T" section. Unlike Case 1, bending moment resistance is a critical limit state for a span of 1.80 m.

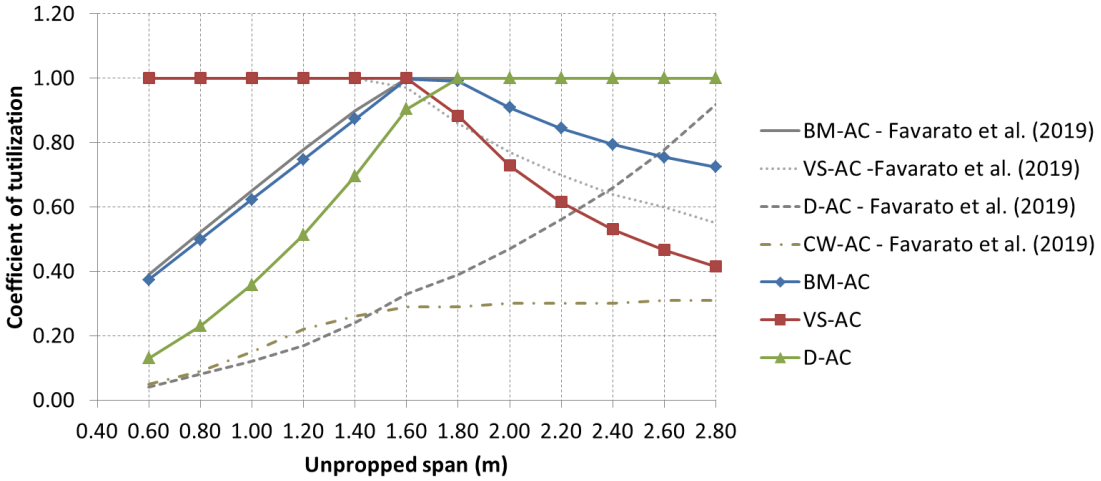

Figure 9. Results for Case 2 – after curing.

The maximum unpropped span, governed by the limit states shown in Figure 10, may present an increase of 80% if buckling of the upper truss bar is taken as failure criteria (from 1.00 m to 1.80 m). Or 100% when buckling of the upper bar is allowed to occur, which places maximum deflection as the governing design parameter during construction (1.00 m to 2.00 m).

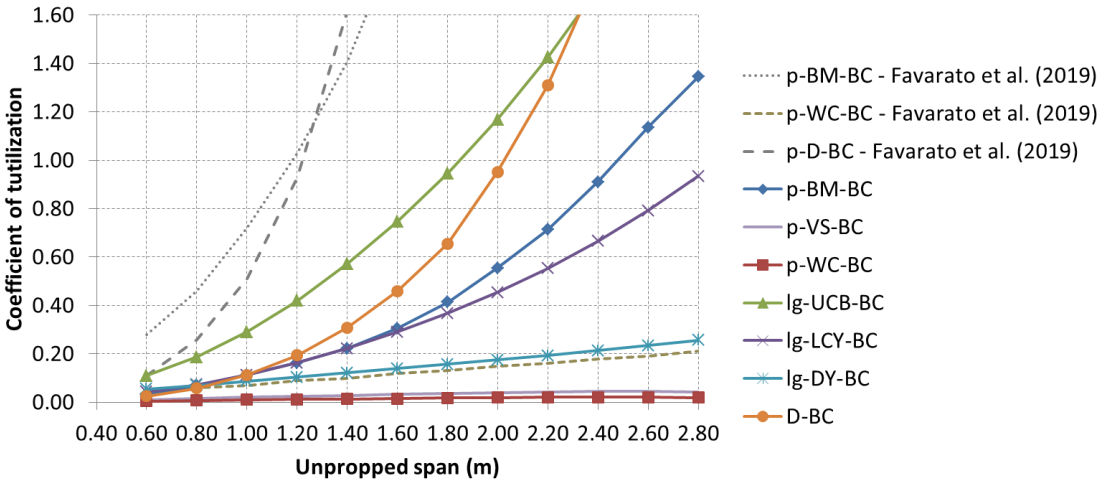

Figure 10. Results for Case 2 – before curing.

Comparison of Cases 1 and 2 allows the expression of maximum live load as a function of unpropped span, shown in Figure 11. It is concluded that a design method that considers the structural contribution provided by the CFS profile also contributes to the ultimate resistance of the slab, since vertical shear is the limiting factor for small and moderate spans.

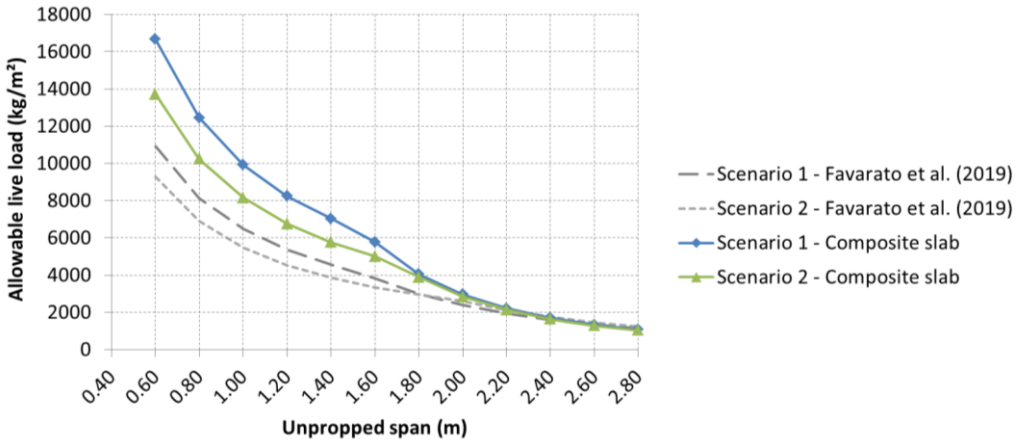

Figure 11. Maximum live loads (characteristic values).

For shorter spans, if the methodology presented herein is compared with the one proposed by FAVARATO et al. (2019), an increment in resistance of 40% and 45% is observed in cases 1 and 2, respectively. This is a result of the shear force resisted by the web of the CFS profile, which is significant when compared to the shear resistance of the concrete and the trussed rebar. For moderate to long spans however, there is a small increase in resistance if the serviceability limit state of excessive deformation is taken as failure criterion. Nonetheless, the increase in flexural rigidity provided by the profile is small in comparison with the flexural rigidity provided by the truss and concrete cross-section. Meaning that even if maximum deflection was not the governing factor, no significant increase in ultimate resistance would be observed.

4 Conclusion

In this paper, a method for the design of steel-concrete composite unidirectional slabs that use CFS stiffened "U" channel profiles was presented. The method accounts for the contribution provided by the CFS profile after curing, and of the combined contribution of CFS profile and trussed rebar during construction. Different geometric and material arrangements may be chosen for this type of slab, which will result in different maximum allowable live loads and maximum unpropped spans.

An analysis of the parametric study conducted shows that accounting for composite behavior in the design procedure did not produce significant increases in the ultimate structural resistance of the slab system, since the significant increase observed is associated with shear force resisted by the profile subjected to minor axis bending.

On the other hand, the equivalence of vertical displacements at the point of introduction of plastic spacers resulted in a significant increase of maximum unpropped span, due to a reduction in maximum deflection. A maximum unpropped span of 2.0 m as observed in this study, makes the Trelifácil system a competitive alternative for the traditional pre-cast lattice girder RC slabs.

References

AHMED, I. M.; TSAVDARIDIS, K. D. The evolution of composite flooring systems: applications, testing, modelling and eurocode design approaches. **Journal of Constructional Steel Research**, v. 155, p. 286–300, 2019. Disponível em: <https://doi.org/10.1016/j.jcsr.2019.01.007>.

ARCELORMITTAL. **Trelifácil®**. Disponível em: <http://longos.arcelormittal.com/produtos/catalogos/trelifacil>. Acesso em: 24 maio 2019.

ASSOCIAÇÃO BRASILEIRA DE NORMAS TÉCNICAS. **NBR 14762 - Dimensionamento de estruturas de aço constituídas por perfis formados a frio**. 2. ed. Rio de Janeiro: [s.n.], 2010.

_____. **NBR 8800 - Projeto de estruturas de aço e de estruturas mistas de aço e concreto de edifícios**. 2. ed. Rio de Janeiro: [s.n.], 2008.

AUSTRALIA, S.; ZEALAND, S. N. **AS/NZS 4600:2005 - Cold-formed steel structures**. [S.l: s.n.], 2005. v. 2005.

BRAUN, M.; HECHLER, O.; BIRARDA, V. 140 m^2 Column Free Space due to Innovative Composite Slim Floor Design. 2009, [S.l: s.n.], 2009. p. 363–368.

COUCHMAN, G.; MULLETT, D.; RACKHAM, J. **Composite Slabs and Beams Using Steel Decking: Best Practice for Design and Construction**. [S.l.]: The Metal Cladding & Roofing Manufacturers Association, 2009.

CRISINEL, M.; O'LEARY, D. Recent Developments in Steel/Concrete Composite Slabs. **Structural Engineering International**, v. 6, n. 1, p. 41–41, 1996.

EN 1991-1-6. **Eurocode 1: Actions on structures - Part 1-6: General actions - Actions during execution**. [S.l: s.n.], 2005. v. 1.

EN 1994-1-1. **Eurocode 4: Design of composite steel and concrete structures - Part 1-1: General rules and rules for buildings**. [S.l: s.n.], 2004. v. 1.

EN1992-1-1. **Eurocode 2: Design of concrete structures - Part 1-1: General rules and rules for buildings**. [S.l: s.n.], 2004. v. 1.

EN1993-1-3. **Eurocode 3: Design of steel structures - Part 1-3: General rules - Supplementary rules for cold-formed members and sheeting**. [S.l: s.n.], 2006. v. 1.

FAVARATO, L. F. et al. Evaluation of the resistance of trussed slabs with steel formwork in cold formed U profile (in press). **Latin American Journal of Solids and Structures**, p. 1–20, 2019. Disponível em: <https://www.lajss.org/index.php/LAJSS/article/view/5304>.

_____. Proposition of a simplified analytical design procedure for lattice girder slabs with shuttering in cold-formed steel lipped channel section. **IBRACON Structural and Materials Journal**, v. In press, 2020.

GASPAR, R. **Análise da Segurança Estrutural das Lajes Pré-Fabricadas Na Fase De Construção**. 1997. 103 f. Universidade de São Paulo, 1997.

GROSSI, L. G. F. **On the structural behavior and the design of composite slabs with additional reinforcement (in Portuguese)**. 2016. 275 f. University of São Paulo, 2016.

INSITUTE, A. I. and S. **S136:16 - North American specification for the design of cold-formed steel structural members**. [S.l: s.n.], 2016.

SIEG, A. P. A. **Study of a slab system with incorporated sheeting (in Portuguese)**. 2015. 143 f. University of São Paulo, 2015.

TAKEY, T. H. **Composite slabs for buildings with incoporated steel sheeting (in Portuguese)**. 2001. 208 f. Pontifícia Universidade Católica do Rio de Janeiro, 2001.

VIANNA, J. C. **Composite slab system for residential constructions using cold formed steel plates with embossments (in Potuguese)**. 2005. 189 f. Pontifícia Universidade Católica do Rio de Janeiro, 2005.